

Continuous and Discrete Variable-Structure Controls for Parallel Three-Phase Boost Rectifier

Sudip K. Mazumder, *Senior Member, IEEE*

Abstract—We describe three nonlinear control schemes for a parallel three-phase boost rectifier consisting of two modules. The basic idea, however, can be extended to a system with N modules. All of the control schemes are developed in a synchronous frame. Moreover, each of the closed-loop power-converter modules operates asynchronously without any communication with the other module. Based on the dynamical equations of the parallel converter, we find that independent control of both of the modules on the dqo axes is not necessary and possible. Consequently, we develop control schemes that stabilize the dq axes and limit the zero-axis disturbance by preventing the flow of the pure zero-sequence current. One of the control schemes is developed purely in the discrete domain. It combines the space-vector modulation scheme with a variable-structure control, thereby keeping the switching frequency constant and achieving satisfactory dynamic performance. The performances of the other control schemes are also satisfactory.

Index Terms—Boost rectifier, parallel converter, space-vector modulation, three phase, variable-structure control, zero-axis disturbance.

I. INTRODUCTION

APPLICATIONS of three-phase power converters are on the rise [2]–[5], [7], [8], [10], [11], [13], [15]–[17] because they provide several advantages including capability to handle high power, modularity, high reliability, less voltage or current ripple, and fast dynamic response. Traditionally, a parallel multiphase converter either has a transformer at the ac side [7], [8], [10] or uses separate power supplies [5]. This approach, however, results in a bulky and expensive system because of the line-frequency transformer and the additional power supplies.

A recent approach to overcome these problems is to directly connect three-phase converters in parallel; one such system is shown in Fig. 1. When two three-phase pulsewidth-modulation (PWM) modules are directly connected, circulating currents can exist in all of the phases [13]. Several methods have been proposed to reduce the cross current among the modules [2]–[4], [12]. Using a linear controller and space-vector modulation (SVM) schemes, which do not use the zero vectors, Xing *et al.* [13] have developed schemes for standardized three-phase modules to reduce the cross current. The advantage of such schemes is that the communication between the modules is minimal. However, the transient response of the parallel three-phase boost rectifier (PTBR) is not satisfactory and the

magnitude of the zero-sequence current under steady-state conditions is not shown. Recently, Ye *et al.* [15] have proposed a linear control scheme¹, which is simple and minimizes the zero-sequence current under steady-state condition by simply varying the duration of the zero space vector. However, if the system saturates, the control scheme will not work effectively, even under steady-state conditions. This is because, when the system saturates, the zero vector can not be applied. Furthermore, the performance of the system under transient conditions has not been demonstrated [15].

II. MODELING AND ANALYSIS OF THE PTBR

We consider a PTBR with two power modules, M1 and M2. Such a PTBR was built by the author at the Center for Power Electronics System (CPES) at Virginia Polytechnic Institute and State University, Blacksburg. Reference [13] and all of the discussion in this paper is based on this system. The parametric details of the power stage are tabulated in Table I. For each module, we assume that the variation in the line inductance of each phase is negligible. However, the line inductances for two different modules are different. We also assume that the equivalent series resistance (ESR) of the output capacitor is negligible and the input voltages are balanced; that is, $v_a + v_b + v_c = 0$. Based on Fig. 1, we obtain the following differential equations, which describe the dynamics of the PTBR:

$$\begin{aligned} \dot{i}_C(t) &= -\frac{1}{C}i_{\text{load}}(t) + \frac{1}{2C} \sum_{k=1}^2 \left(\sum_{j=1}^3 i_{L_{kj}}(t) u_{kj}(t) \right) \\ \dot{i}_{L_k}^{abc}(t) &= (P_{k1} + P_{k2}) \vec{i}_{L_k}^{abc}(t) + P_{k3} V^{abc}(t) \\ &\quad + P_{k4} \vec{u}_1^{abc}(t) v_C(t) + P_{k5} \vec{u}_2^{abc}(t) v_C(t). \end{aligned} \quad (1)$$

In (1) and for the rest of the paper, $k = 1$ and 2 ; further, we will drop the notation time (t) for the rest of the paper. The vectors representing the phase currents and switching functions of M1 and M2 are given by

$$\begin{aligned} \vec{i}_{L_k}^{abc}(t) &= (i_{L_{k1}}(t) \quad i_{L_{k2}}(t) \quad i_{L_{k3}}(t))^T \\ \vec{u}_k^{abc}(t) &= (u_{k1}(t) \quad u_{k2}(t) \quad u_{k3}(t))^T \\ \vec{V}^{abc} &= (v_a \quad v_b \quad v_c)^T \end{aligned}$$

and the matrices P_{ki} ($i = 1, 2, \dots, 5$) are given in the Appendix. For the PTBR, the top and bottom switches of any phase are complementary in nature. The switching functions u_{kj} ($i = 1, 2, 3$) attain a value of

¹In this paper, we will refer to this control proposed by Ye [15] as CS_{LINEAR} .

Manuscript received November 26, 2003; revised February 18, 2004. Abstract published on the Internet January 13, 2005. This work was supported in part by National Science Foundation CAREER Award 0239131.

The author is with the Laboratory for Energy and Switching-Electronics Systems, Department of Electrical and Computer Engineering, University of Illinois, Chicago, IL 60607 USA (e-mail: mazumder@ece.uic.edu).

Digital Object Identifier 10.1109/TIE.2005.843921

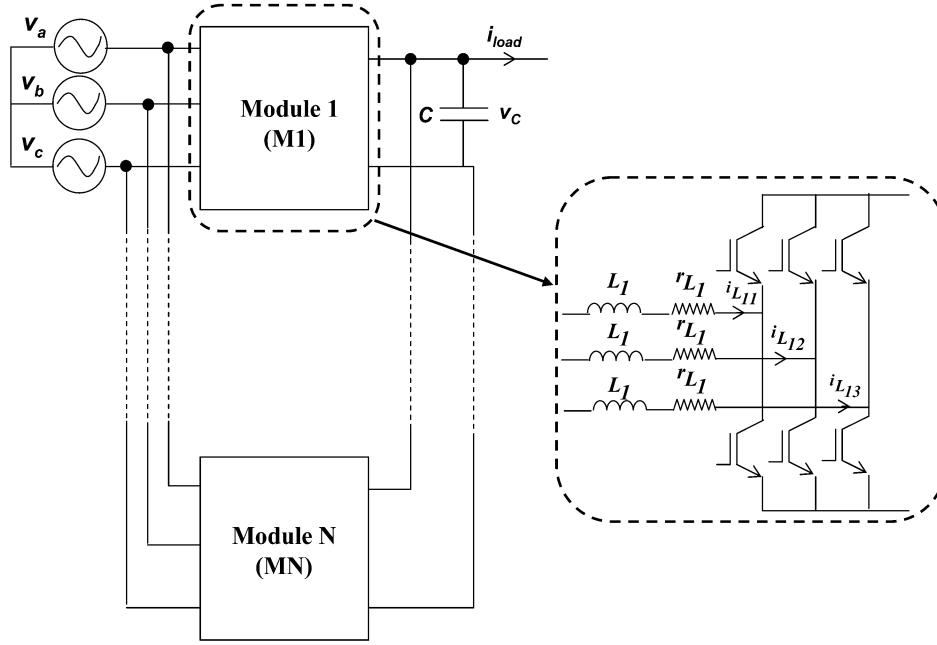
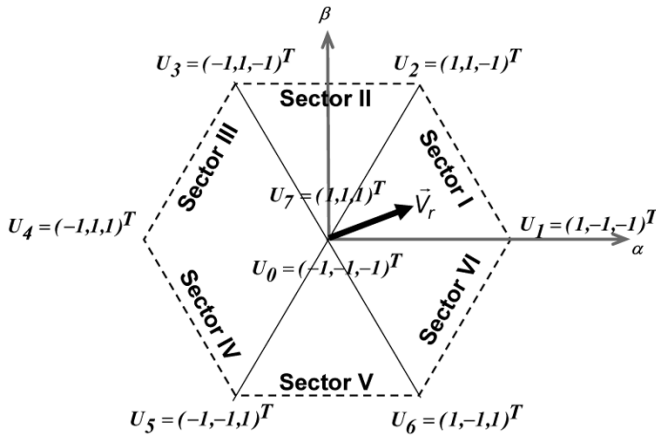

 Fig. 1. Schematic of a PTBR with N modules.

 TABLE I
 NOMINAL PARAMETERS OF THE PTBR

Parameter	Nominal Values
$v_{ab} = v_{bc} = v_{ca} = v_n$	208 V (rms)
v_C (regulated)	400 V
Nominal switching frequency ($= 1/T$)	32 kHz
$L_1 = L_2 = L_n$	500 μ H
$r_{L1} = r_{L2} = r_{L_n}$	0.5 Ω
Bus capacitance (C)	1200 μ F
Load resistance (R)	4 Ω
Power ratings of M1 and M2	20 kVA


 Fig. 2. Distribution of the space vectors in the $\alpha\beta$ frame.

-1 (or 1) if the bottom (or top) switch of any phase is on. For the PTBR, and as shown in Fig. 2, \vec{u}_1^{abc} and \vec{u}_2^{abc} can attain only eight discrete values (space vectors)— $U_0(-1, -1, -1)^T$, $U_1(1, -1, -1)^T$, $U_2(1, 1, -1)^T$,

$U_3(-1, 1, -1)^T$, $U_4(-1, 1, 1)^T$, $U_5(-1, -1, 1)^T$, $U_6(1, -1, 1)^T$, and $U_7(1, 1, 1)^T$ —for feasible operation. Two of these U_0 and U_7 are the zero vectors, while the other six are the active vectors.

Next, using the generic transformation [12]

$$\vec{X}^{abc} = [T(\theta)]^{-1} \vec{X}^{dqo} = [T(\theta)]^{-1} [x_d \ x_q \ x_o]^T \quad (2)$$

where x_d , x_q , and x_o are referred to as the active, reactive, and the zero-axis components and $[T(\theta)]^{-1}$ is a nonsingular matrix [17], and $\theta = \theta(t_0) + \int_0^t \omega d\tau$ (where ω is the line angular frequency), we rewrite (1) as

$$\begin{aligned} \dot{v}_C &= -\frac{1}{C} i_{load}(t) + \frac{1}{2C} (i_{L_{kd}} u_{kd} + i_{L_{kq}} u_{kq} + i_{L_{ko}} u_{ko}) \\ \dot{i}_{L_k}^{dqo} &= T(\theta)(P_{k1} + P_{k2})(T(\theta))^{-1} \dot{i}_{L_k}^{dqo} \\ &\quad + T(\theta)P_{k3}(T(\theta))^{-1} \vec{V}^{dqo} + T(\theta)P_{k4}(T(\theta))^{-1} \vec{u}_1^{dqo} \\ &\quad + T(\theta)P_{k5}(T(\theta))^{-1} \vec{u}_2^{dqo} - T(\theta) \frac{d}{dt} (T(\theta))^{-1} \dot{i}_{L_k}^{dqo}. \end{aligned} \quad (3)$$

In (3), $\vec{i}_{L_k}^{dqo} = (i_{L_{kd}} \ i_{L_{kq}} \ i_{L_{ko}})^T$, $\vec{V}^{dqo} = (v_d \ v_q \ v_o)^T$, $\vec{u}_k^{dqo} = (u_{kd} \ u_{kq} \ u_{ko})^T$, and $v_q = v_o = 0$ (because we have assumed that the line voltages are balanced). Using [17], we simplify (3) to

$$\begin{aligned} \dot{v}_C &= -\frac{1}{C} i_{load}(t) + \frac{1}{2C} (i_{L_{kd}} u_{kd} + i_{L_{kq}} u_{kq} + i_{L_{ko}} u_{ko}) \\ \dot{i}_{L_k}^{dqo} &= \begin{pmatrix} \dot{i}_{L_{kd}} \\ \dot{i}_{L_{kq}} \\ \dot{i}_{L_{ko}} \end{pmatrix} = \begin{pmatrix} -\frac{r_{Lk}}{L_k} & \omega & 0 \\ \omega & -\frac{r_{Lk}}{L_k} & 0 \\ 0 & 0 & -\frac{r_{L1}+r_{L2}}{L_1+L_2} \end{pmatrix} \begin{pmatrix} i_{L_{kd}} \\ i_{L_{kq}} \\ i_{L_{ko}} \end{pmatrix} \\ &\quad + \frac{1}{L_k} \begin{pmatrix} v_d \\ v_q \\ v_o \end{pmatrix} - \frac{v_C}{2L_k} \begin{pmatrix} 1 & 0 & 0 \\ 0 & 1 & 0 \\ 0 & 0 & \frac{L_k}{L_1+L_2} \end{pmatrix} \begin{pmatrix} u_{kd} \\ u_{kq} \\ u_{ko} \end{pmatrix} - \delta_k \end{aligned} \quad (4)$$

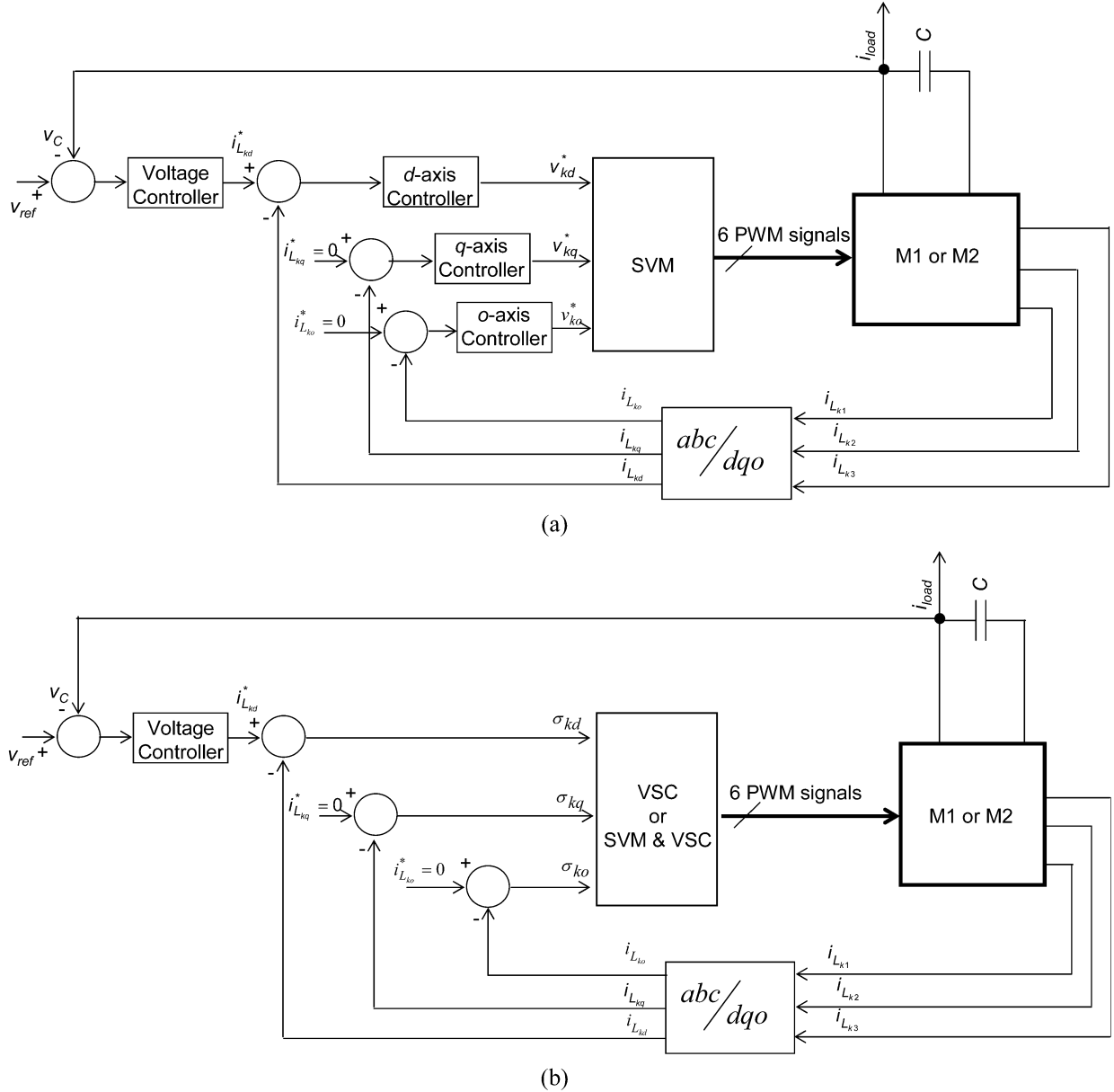


Fig. 3. Overall control architectures for the PTBR with modules M1 and M2. (a) dq - or dqo -axes controllers representing a conventional controller [12], [13] and CS_{LINEAR} [15]. (b) Controller structure for CS_{CONT1} or CS_{CONT2} or CS_{DISCRETE} . For CS_{DISCRETE} , the feedback signals are sampled. Note that because M1 and M2 are both connected to the same bus, they have a common bus voltage; additionally, all the feedback signals are, “in reality,” the outputs of voltage and current sensors.

where δ_k is a disturbance term representing

$$\delta_1 = \frac{v_C}{2L_1} \begin{pmatrix} 0 & 0 & -\frac{L_1}{L_1 + L_2} u_{2o} \end{pmatrix}^T$$

and

$$\delta_2 = \frac{v_C}{2L_2} \begin{pmatrix} 0 & 0 & -\frac{L_2}{L_1 + L_2} u_{1o} \end{pmatrix}^T$$

for M1 and M2, respectively. Equation (4) shows that, for each module, the dynamical equations governing the currents on the dq axes depend only on u_{1d} (or u_{2d}) and u_{1q} (or u_{2q}). The differential equations describing the zero-axis currents involve a cross-coupling control term.

III. CONTROL SCHEMES

As shown in Fig. 3, the controllers for M1 and M2 have a multiloop structure, with an outer voltage loop and an inner current loop. The control concept developed in this paper extends to more than two modules ($N > 2$). The current loops are designed to be fast so that the closed-loop system can reject the feedforward and feedback disturbances and regulate the output voltage. The outer voltage loop is designed to be slow and is based on a linear lag-lead controller with an integrator [12]. The objectives of the control are threefold. First, we want to regulate the bus voltage at 400 V. Second, the phase currents of each module should be synchronous with the input phase voltages. Third, M1 and M2 should share the power consumed by the load

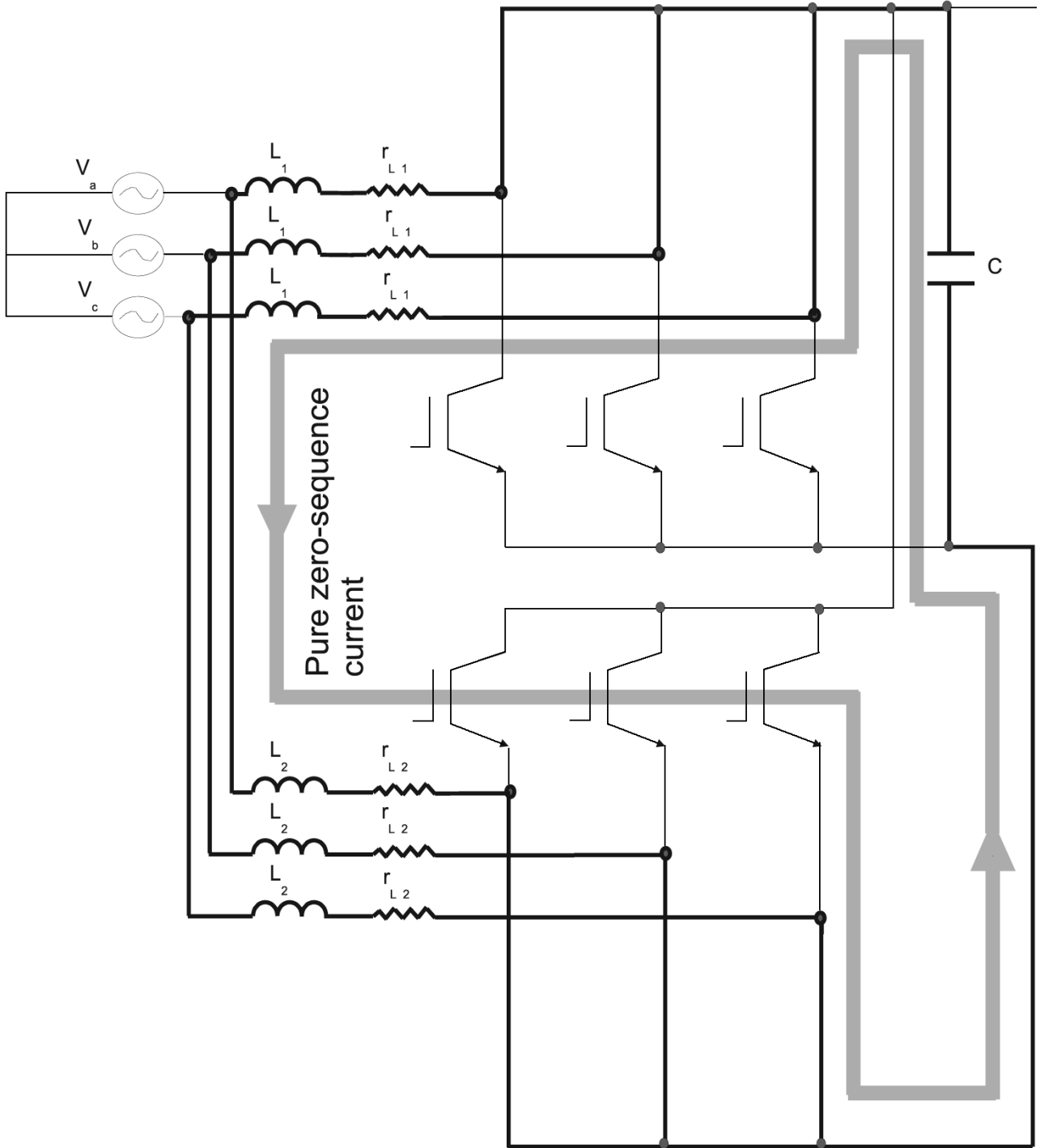


Fig. 4. Path of the pure zero-sequence current in the PTBR.

equally. However, these objectives have to be met by controlling M1 and M2 as independently as possible. The only common feedback to both the modules is the d -axis reference current (i_{Lkd}^*) obtained from the outer voltage loop, which serves as the master. We use a common voltage loop because both M1 and M2 are connected over a common dc bus. The q -axis (i_{Lkq}^*) and the o -axis (i_{Lko}^*) reference currents are maintained equal to zero to obtain unity-power-factor operation and minimize the zero-axis interaction between the two modules.

Based on these control objectives and structure, we develop three control schemes in the following sections. While the

first two control schemes (CS_{CONT1} and CS_{CONT2}) are synthesized in the continuous domain, the third control scheme ($CS_{DISCRETE}$) is developed in the discrete domain. The nominal switching frequency of M1 and M2 is set at 32 kHz, to emulate the actual system [13]. We, however, test the control when the modules are not synchronized and their switching frequencies are different.

A. Continuous Control Scheme One: (CS_{CONT1})

Equation (4) shows that the open-loop PTBR is a seventh-order dynamical system. There are two sets of three differential

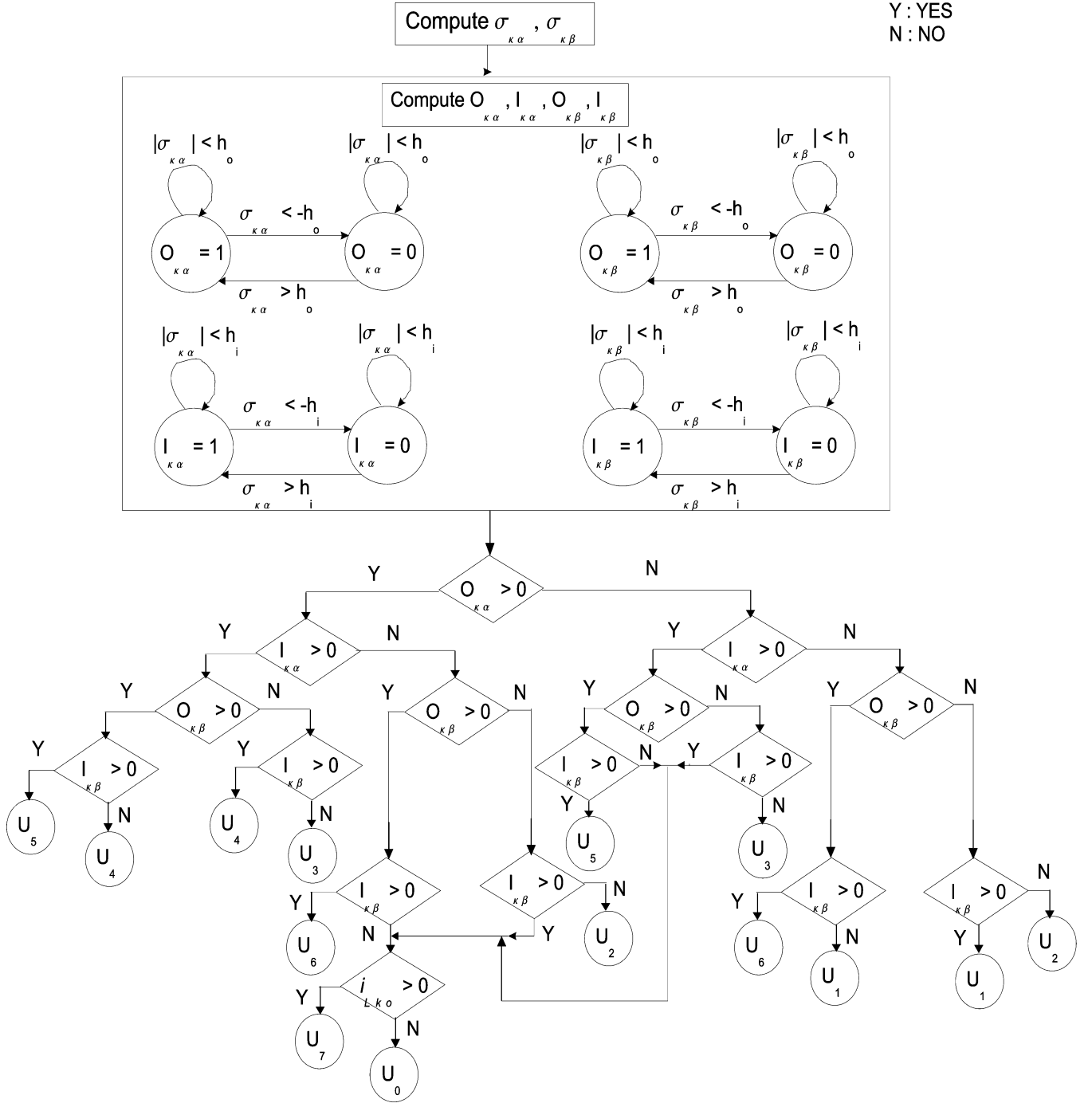


Fig. 5. Flowchart for the implementation of the control scheme CS_{CONT2} .

equations that describe the dynamics of the current for M1 and M2 on the dqo axes and one additional differential equation for describing the dynamics of the bus voltage. One approach for implementing the current loops of M1 and M2 independently is to define the following six sliding surfaces:

$$\begin{aligned} \sigma_{kd} &= i_{Lkd}^* - i_{Lkd} = 0, & \sigma_{kq} &= i_{Lkq}^* - i_{Lkq} = 0, \\ \sigma_{ko} &= i_{Lko}^* - i_{Lko} = 0 \end{aligned} \quad (5)$$

and synthesize controls that will reduce $\|\sigma_{kd} + \sigma_{kq} + \sigma_{ko}\|$ to zero. However, the rank of the control matrix $(\dot{i}_{L1}^{dqo} \ \dot{i}_{L2}^{dqo})^T$ in $(i_{L1}^{dqo} \ i_{L2}^{dqo})^T$ is five; thus, it is impossible to control all of the

six currents (\dot{i}_{L1}^{dqo} and \dot{i}_{L2}^{dqo}) independently. One way to avoid the redundancy problem is to control the sliding manifold

$$(\sigma_{1d} = 0) \cap (\sigma_{1q} = 0) \cap (\sigma_{1o} = 0) \cap (\sigma_{2d} = 0) \cap (\sigma_{2q} = 0) \cdots \quad (6)$$

To consider the stability of the sliding manifold (6), we define a positive-definite Lyapunov function

$$V(\sigma_{1d}, \sigma_{1q}, \sigma_{1o}, \sigma_{2d}, \sigma_{2q}) = \frac{1}{2} (\sigma_{1d}^2 + \sigma_{1q}^2 + \sigma_{1o}^2 + \sigma_{2d}^2 + \sigma_{2q}^2) \quad (7)$$

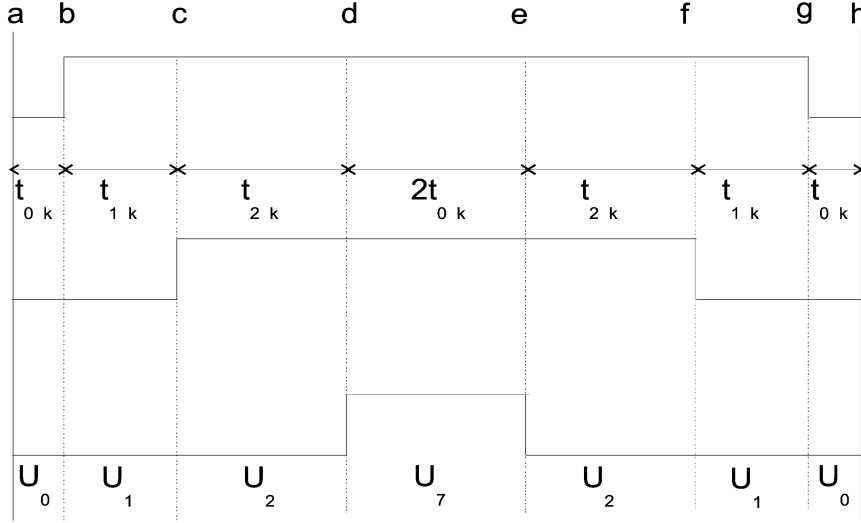


Fig. 6. A sample space-vector-modulated waveform to synthesize the reference voltage vector in Sector I.

which has a quadratic form. For the manifold to be stable

$$\begin{aligned} \dot{V}(\sigma_{1d}, \sigma_{1q}, \sigma_{1o}, \sigma_{2d}, \sigma_{2q}) \\ = \sigma_{1d}\dot{\sigma}_{1d} + \sigma_{1q}\dot{\sigma}_{1q} + \sigma_{1o}\dot{\sigma}_{1o} + \sigma_{2d}\dot{\sigma}_{2d} + \sigma_{2q}\dot{\sigma}_{2q} < 0. \end{aligned} \quad (8)$$

Using [9], [17], we can show that $\sigma_{kd}\dot{\sigma}_{kd} < 0$ and $\sigma_{kq}\dot{\sigma}_{kq} < 0$ provided

$$\begin{aligned} u_{kd} &= -\gamma_{kd}\text{sgn}(\sigma_{kd}) \quad \text{where } |\gamma_{kd}| \\ &> \left| \dot{i}_{L_{kd}}^* + \frac{rL_k}{L_k}i_{L_{kd}} - \omega i_{L_{kq}} - \frac{1}{L_k}v_d + \frac{v_C}{2L_k}u_{kd} \right| \frac{2L_k}{v_C} \\ u_{kq} &= -\gamma_{kq}\text{sgn}(\sigma_{kq}) \quad \text{where } |\gamma_{kq}| \\ &> \left| \dot{i}_{L_{kq}}^* + \frac{rL_k}{L_k}i_{L_{kq}} - \omega i_{L_{kd}} - \frac{1}{L_k}v_q + \frac{v_C}{2L_k}u_{kq} \right| \frac{2L_k}{v_C}. \end{aligned} \quad (9)$$

However, it is not possible to satisfy $\sigma_{1o}\dot{\sigma}_{1o} < 0$ using a single space vector in a single switching cycle because of the zero-axis disturbance [16]. This eliminates the possibility of satisfying (8) for all values of σ , but depending on the values of σ_{kd} , σ_{kq} , and σ_{1o} , we can always establish a bound beyond which (8) holds [16]. This bound is minimized if the zero-axis disturbance is reduced. A quick look at $\dot{i}_{L_{1o}}$ shows that the zero-axis disturbance is reduced by increasing the size of the line inductors or the switching frequency because u_{2o} depends on the switching vectors. However, we cannot increase either of them arbitrarily to avoid making the converter bulky and inefficient.

For the PTBR, as shown in Fig. 4, the worst disturbance occurs when $\vec{u}_1^{abc} = U_7$ and $\vec{u}_2^{abc} = U_0$ and vice-versa. During this switching configuration a pure zero-axis current flows from M1 to M2 or vice-versa that is not reflected on the dq axes. This is because the path of this zero-sequence current involves the output capacitor, the top (or bottom) switches of M1 and M2. Therefore, if we eliminate this possible switching configuration, then we can reduce the impact of the disturbance significantly. Although the zero-axis disturbance exists for other switching

configurations, it is reflected on the dq axes, and hence the impact of this disturbance can be minimized by having a fast current loop on the dq axes [13], [15], [17].

Thus, the control strategy for CS_{CONT1} is as follows: we control σ_{kd} and σ_{kq} using (9) and limit the zero-axis disturbance (by selecting proper u_{ko} depending on the value of $i_{L_{ko}}$ [16]), thereby preventing the flow of the zero-axis current from M1 to M2 or vice-versa. Then, using the transformation (2), we transform the controls in the dqo axes to the abc axes.

B. Continuous Control Scheme Two: (CS_{CONT2})

The second scheme is a variation of the first scheme. A similar scheme is outlined in [14] for control of a single multiphase converter. However, it does not address the problem of zero-axis disturbance, which is a key issue in the stabilization of a PTBR. The second scheme uses hysteresis to control the switching frequency. First, we compute σ_{kd} and σ_{kq} using (5) and then transform the errors to the $\alpha\beta$ coordinates using

$$\begin{pmatrix} \sigma_{k\alpha} \\ \sigma_{k\beta} \end{pmatrix} = \begin{pmatrix} \cos(\theta) & -\sin(\theta) \\ \sin(\theta) & \cos(\theta) \end{pmatrix} \begin{pmatrix} \sigma_{kd} \\ \sigma_{kq} \end{pmatrix} \quad (10)$$

where $\theta = \theta(t_0) + \int_0^t \omega d\tau$. The selection of the switching vectors is such that

$$\sigma_{k\alpha}\dot{\sigma}_{k\alpha} < 0, \quad \sigma_{k\beta}\dot{\sigma}_{k\beta} < 0, \quad \text{and } \|\sigma_{1o}\| \text{ is bound} \quad (11)$$

for a given frequency and inductor size. The last condition in (11) is achieved by using an appropriate zero vector based on the direction of $i_{L_{ko}}$. For example, if $i_{L_{ko}} < 0$ and the space vector needed to satisfy $\sigma_{1\alpha}\dot{\sigma}_{1\alpha} < 0$ and $\sigma_{1\beta}\dot{\sigma}_{1\beta} < 0$ is U_7 , then we implement U_0 instead. This simple change will not affect the stability of the sliding surfaces on the $\alpha\beta$ axes, but will reduce the zero-axis disturbance [16]. In addition, to achieve a compromise between the transient response and the harmonic distortion, we use a two-level hysteric comparator (for each axis), which has two thresholds (h_i and h_o).

Fig. 5 shows a flowchart that illustrates the procedure for selecting the appropriate switching vector for either M1 or M2. *The advantage of CS_{CONT2} is that we can limit the switching frequency and keep a balance between the distortion of the line currents and the transient response.* Although the pure zero-sequence current is eliminated, the impact of the overall zero-sequence disturbance is still determined by the switching frequency and the inductor size.

C. Discrete Control Scheme (CS_{DISCRETE})

We look for stability on a reduced-order manifold, where instead of controlling u_{1o} - u_{2o} (or u_{2o} - u_{1o}), we control their averages; that is, \bar{u}_{1o} - \bar{u}_{2o} (or \bar{u}_{2o} - \bar{u}_{1o}). The proposed discrete variable-structure control (VSC) scheme (CS_{DISCRETE}), unlike the CS_{CONT1} and CS_{CONT2}, keeps the switching frequency constant by combining VSC with SVM techniques. The discrete VSC scheme can be combined with any SVM scheme. However, not all of the SVM techniques can be used to reject the disturbance due to the zero-axis currents [15]. Therefore, we choose the SVM scheme outlined in [13], [17] to control the zero-axis current. In any given switching cycle, this SVM scheme synthesizes a reference voltage vector (\vec{v}_r) (see Fig. 2) using two zero vectors and two active vectors. For example, if \vec{v}_r is in Sector I, then it is synthesized as $\vec{v}_r = (v_C)/(2T)(t_1U_0 + t_2U_1 + t_3U_2 + t_4U_7 + t_5U_2 + t_6U_1 + t_7U_0)$, where $T = t_1 + t_2 + t_3 + t_4 + t_5 + t_6 + t_7$ is the switching time period. Having selected the SVM scheme, we need to express $i_{L_{kd}}$ and $i_{L_{kq}}$ in discrete form to implement the current loop using the discrete VSC. The discrete form of $i_{L_k}^{dq}$ is a map of the form $i_{L_k}^{dq}(n+1) = F_k(i_{L_k}^{dq}(n), \vec{V}^{dq}(n), \vec{t}_k^{dq}(n))$, where $i_{L_k}^{dq} = [i_{L_{kd}} \ i_{L_{kq}}]^T$, $\vec{V}^{dq} = [v_d \ v_q]^T$, and $\vec{t}_k^{dq} = [t_{kd} \ t_{kq}]^T$.

To obtain this map, we first solve for $i_{L_k}^{dq}$ using (4) in each time interval of the SVM waveform [17]. One such waveform is shown in Fig. 6, which is valid only for Sector I. We start by solving for $i_{L_{kd}}$ and $i_{L_{kq}}$ in Sector I for each interval of time. Once we obtain all of the solutions, we obtain a map that relates $i_{L_{kd}}$ and $i_{L_{kq}}$ at the end of a switching cycle with those at the beginning. Subsequently, using this map, which is valid only for Sector I, we obtain the generalized map for $i_{L_k}^{dq}(n+1)$. Fig. 6 shows that, although there are seven intervals of time in a given switching cycle, only three of them are distinct. The maps

for each of these three distinct intervals are described by (12), shown at the bottom of the page, (14), and (15), [17].

If a quasi-static assumption (i.e., the variation of θ in each switching cycle is negligible) is made, then (13), shown at the bottom of the page, is reduced to the following [17]:

$$\begin{aligned} i_{L_k}^{dq}(m+1) &= e^{A_k t_{1k}} i_{L_k}^{dq}(m) + (e^{A_k t_{1k}} - I) A_k^{-1} B_k \vec{V}^{dq} \\ &\quad + ((e^{A_k t_{1k}} - I) A_k^{-1} C_{k1} \cos(\theta(n)) \\ &\quad + (e^{A_k t_{1k}} - I) A_k^{-1} C_{k2} \sin(\theta(n))) v_C(n) \\ &= \Phi_{k2} i_{L_k}^{dq}(m) + \Gamma_{k2} \vec{V}^{dq} + \Omega_{k2} v_C(n). \end{aligned} \quad (14)$$

(in the intervals b–c and f–g).

The form of the map for the third distinct interval (c–d and e–f) is identical to that of (14)

$$\begin{aligned} i_{L_k}^{dq}(m+1) &= e^{A_k t_{2k}} i_{L_k}^{dq}(m) + (e^{A_k t_{2k}} - I) A_k^{-1} B_k \vec{V}^{dq} \\ &\quad + ((e^{A_k t_{2k}} - I) A_k^{-1} D_{k1} \cos(\theta(n)) \\ &\quad + (e^{A_k t_{2k}} - I) A_k^{-1} D_{k2} \sin(\theta(n))) v_C(n) \\ &= \Phi_{k3} i_{L_k}^{dq}(m) + \Gamma_{k3} \vec{V}^{dq} + \Omega_{k3} v_C(n). \end{aligned} \quad (15)$$

(in the intervals c–d and e–f).

In (12)–(15), m represents the m th subsampling period in the n th sampling period, $i_{L_k}^{dq}(m)$ is the initial value of $i_{L_k}^{dq}$ at the beginning of the subinterval, and t_{0k} , t_{1k} , and t_{2k} are the durations of the subintervals outlined in (12)–(15) and as illustrated in Fig. 6. All other matrices are described in [17]. Using (12), (14), and (15) and knowing that $t_{3k} = 2t_{0k}$, $t_{5k} = t_{1k}$, $t_{4k} = t_{2k}$, $t_{7k} = t_{0k}$; $\Omega_{k1} = \Omega_{k4} = \Omega_{k7} = 0$; $\Omega_{k2} = \Omega_{k6}$; $\Omega_{k3} = \Omega_{k5}$, we obtain the map [17]

$$\begin{aligned} i_{L_k}^{dq}(n+1) &= \Phi_k i_{L_k}^{dq}(n) + \Gamma_k \vec{V}^{dq} + \Omega_{ka} t_{k1}(n) v_C(n) \\ &\quad + \Omega_{kb} t_{k2}(n) v_C(n) \end{aligned} \quad (16)$$

where $\Phi_k = e^{A_k T}$, $\Gamma_k = (e^{A_k T} - I) A_k^{-1} B_k$, $\Omega_{ka} = 2C_{k1} \cos(\theta(n)) + 2C_{k2} \sin(\theta(n))$, and $\Omega_{kb} = 2D_{k1} \cos(\theta(n)) + 2D_{k2} \sin(\theta(n))$. Using

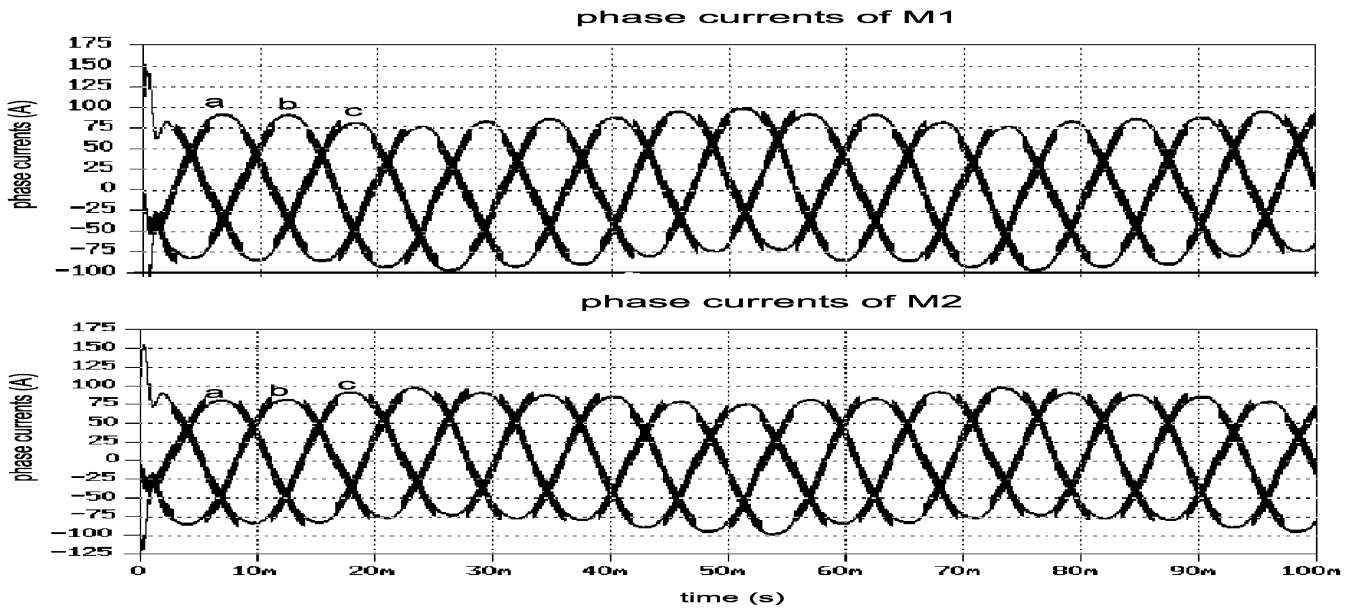
$$\begin{aligned} t_{kd} &= \frac{1}{2}(\cos(\theta) + \sqrt{3}\sin(\theta))2t_{2k} + \cos(\theta)2t_{1k}; \\ t_{kq} &= \frac{1}{2}(\sqrt{3}\cos(\theta) - \sin(\theta))2t_{2k} - \sin(\theta)2t_{1k} \end{aligned} \quad (17)$$

$$\begin{aligned} i_{L_k}^{dq}(m+1) &= e^{A_k t_{0k}} i_{L_k}^{dq}(m) + (e^{A_k t_{0k}} - I) A_k^{-1} B_k \vec{V}^{dq} \\ &= \Phi_{k1} i_{L_k}^{dq}(m) + \Gamma_{k1} \vec{V}^{dq} + \Omega_{k1} v_C(n) \end{aligned} \quad (12)$$

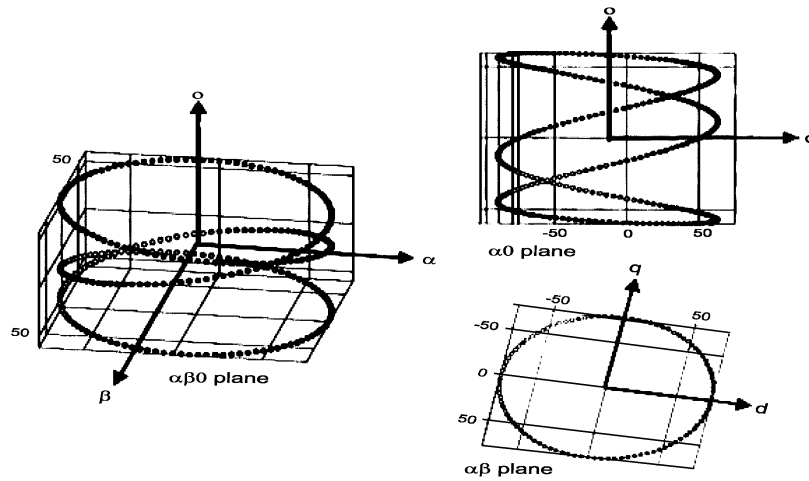
(in the intervals a–b, g–h, and half of d–e)

$$\begin{aligned} i_{L_k}^{dq}(m+1) &= e^{A_k t_{1k}} i_{L_k}^{dq}(m) + (e^{A_k t_{1k}} - I) A_k^{-1} B_k \vec{V}^{dq} \\ &\quad + v_C(n) \left(\begin{aligned} &\left(\frac{e^{i\omega(t_k(m)+t_{1k})}}{2} M_k (e^{(\Lambda_k - i\omega I)t_{1k}} - I) (\Lambda_k - i\omega I)^{-1} M_k^{-1} C_{k1} \right) \\ &\left(\frac{e^{-i\omega(t_k(m)+t_{1k})}}{2} M_k (e^{(\Lambda_k + i\omega I)t_{1k}} - I) (\Lambda_k + i\omega I)^{-1} M_k^{-1} C_{k1} \right) \\ &+ \left(\frac{e^{i\omega(t_k(m)+t_{1k})}}{2i} M_k (e^{(\Lambda_k - i\omega I)t_{1k}} - I) (\Lambda_k - i\omega I)^{-1} M_k^{-1} C_{k2} \right. \\ &\quad \left. + \frac{e^{-i\omega(t_k(m)+t_{1k})}}{2i} M_k (e^{(\Lambda_k + i\omega I)t_{1k}} - I) (\Lambda_k + i\omega I)^{-1} M_k^{-1} C_{k2} \right) \end{aligned} \right). \end{aligned} \quad (13)$$

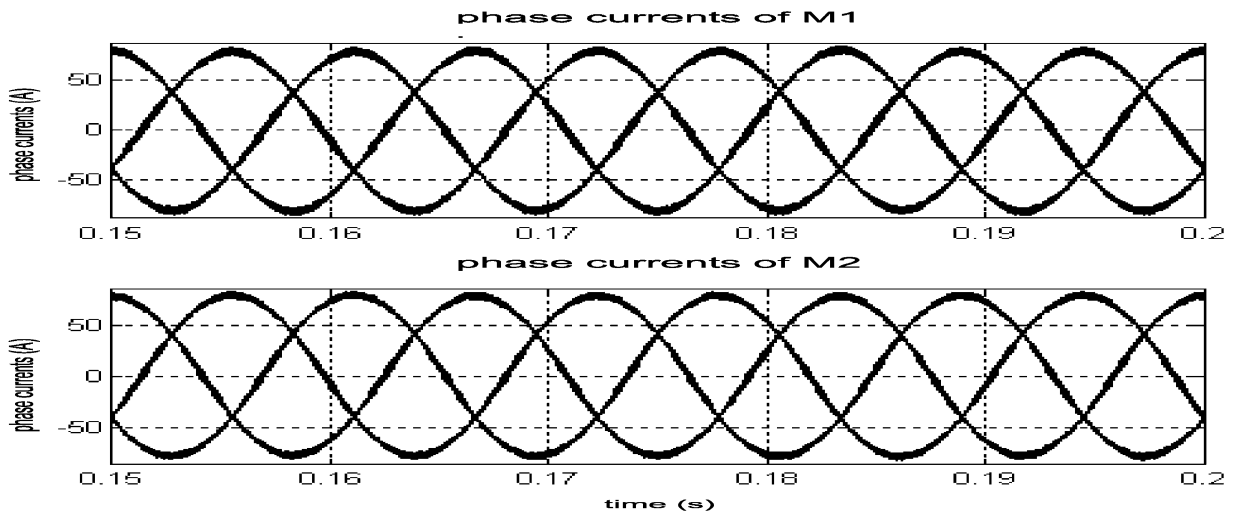
(in the intervals b–c and f–g)



(a)



(b)



(c)

Fig. 7. (a) The phase currents of M1 and M2 using a conventional dq controller when the parameters of the modules are the same, except L_1 is 95% of L_2 . (b) Three-dimensional view of the unbalanced phase currents of M1 in the $\alpha\beta o$ frame. (c) The phase currents of M1 and M2 obtained using CS_{LINEAR} when the parameters of the modules are the same, except L_1 is 95% of L_2 .

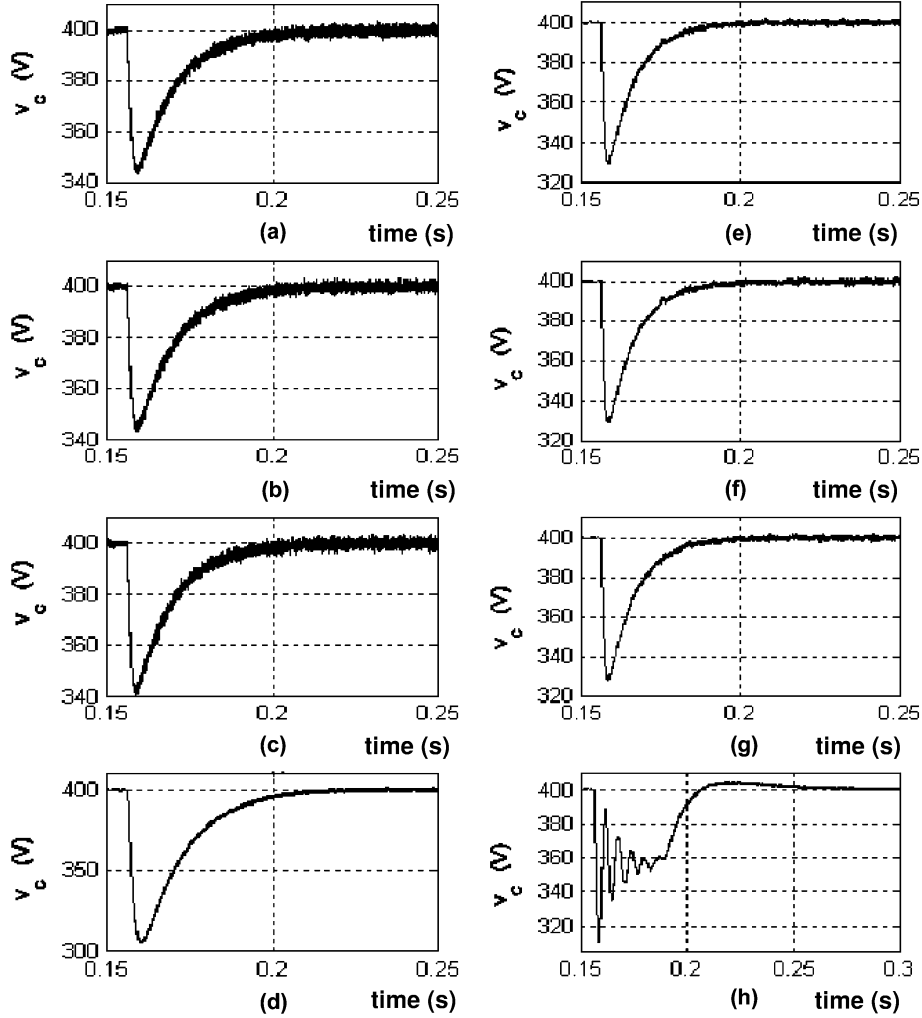


Fig. 8. Change in the bus voltage obtained using CS_{CONT1} (a), (e), CS_{CONT2} (b), (f), CS_{DISCRETE} (c), (g), and CS_{LINEAR} (d), (h) for *case 1* (figures on the left) and *case 2* (figures on the right).

we convert (16) to the following form:

$$\begin{aligned} \vec{i}_{L_k}^{dq}(n+1) &= F_k \left(\vec{i}_{L_k}^{dq}(n), \vec{V}^{dq}(n), \vec{t}_k^{dq}(n) \right) \\ &= \Phi_k \vec{i}_{L_k}^{dq}(n) + \Gamma_k \vec{V}^{dq} + \Omega_k \vec{t}_k^{dq}(n) \end{aligned} \quad (18)$$

where Ω_k is a diagonal matrix and we have assumed that the variation of v_C (due to a slower voltage loop) is negligible compared to $\vec{i}_{L_k}^{dq}$ in one switching cycle. Using the procedure described above, we obtain maps similar to (18) for Sectors II–VI.

Now that we have obtained the discrete form of $\vec{i}_{L_k}^{dq}$, we define the following sliding surfaces to control the currents on the dq axes:

$$\begin{aligned} \vec{\sigma}_k^{dq}(n) &= \vec{i}_k^{*dq}(n) - \vec{i}_k^{dq}(n) \\ \text{where } \vec{\sigma}_k^{dq}(n) &= (\sigma_{kd}(n) \quad \sigma_{kq}(n))^T. \end{aligned} \quad (19)$$

The stability of the sliding surfaces $\vec{\sigma}_k^{dq}(n)$ is determined using the discrete Lyapunov function

$$V(\sigma_{kd}(n), \sigma_{kq}(n)) = \frac{1}{2} \left(\vec{\sigma}_k^{dq}(n) \right)^T \vec{\sigma}_k^{dq}(n). \quad (20)$$

For stability [16],

$$\begin{aligned} V_{k+1}(\sigma_{kd}(n+1), \sigma_{kq}(n+1)) - V_k(\sigma_{kd}(n), \sigma_{kq}(n)) &\leq 0 \\ \Rightarrow \sigma_{kd}(n)(\sigma_{kd}(n+1) - \sigma_{kd}(n)) & \\ + \sigma_{kq}(n)(\sigma_{kq}(n+1) - \sigma_{kq}(n)) &\leq 0. \end{aligned} \quad (21)$$

Because Ω_k , in (18), is a diagonal matrix [17], the sliding surfaces $\sigma_{kd}(n)$ and $\sigma_{kq}(n)$ have independent control, the stability condition (21) is simplified to

$$\left(\vec{\sigma}_k^{dq}(n) \right)^T \left(\vec{\sigma}_k^{dq}(n+1) - \vec{\sigma}_k^{dq}(n) \right) \leq 0. \quad (22)$$

Condition (22) is satisfied if we chose

$$\vec{\sigma}_k^{dq}(n+1) - \vec{\sigma}_k^{dq}(n) = (-\lambda_{kd} \text{sgn}(\sigma_{kd}(n)) - \lambda_{kq} \text{sgn}(\sigma_{kq}(n)))^T \vec{\sigma}_k^{dq}(n) \quad (23)$$

and determine $\vec{t}_k^{dq}(n)$ based on (23). In (23), λ_{kd} and λ_{kq} are scalar parameters that determine how fast the closed-loop system reaches the quasi-sliding surface. Substituting (19) into (23), and expanding (18), we obtain

$$\vec{\sigma}_k^{dq}(n+1) - \vec{\sigma}_k^{dq}(n)$$

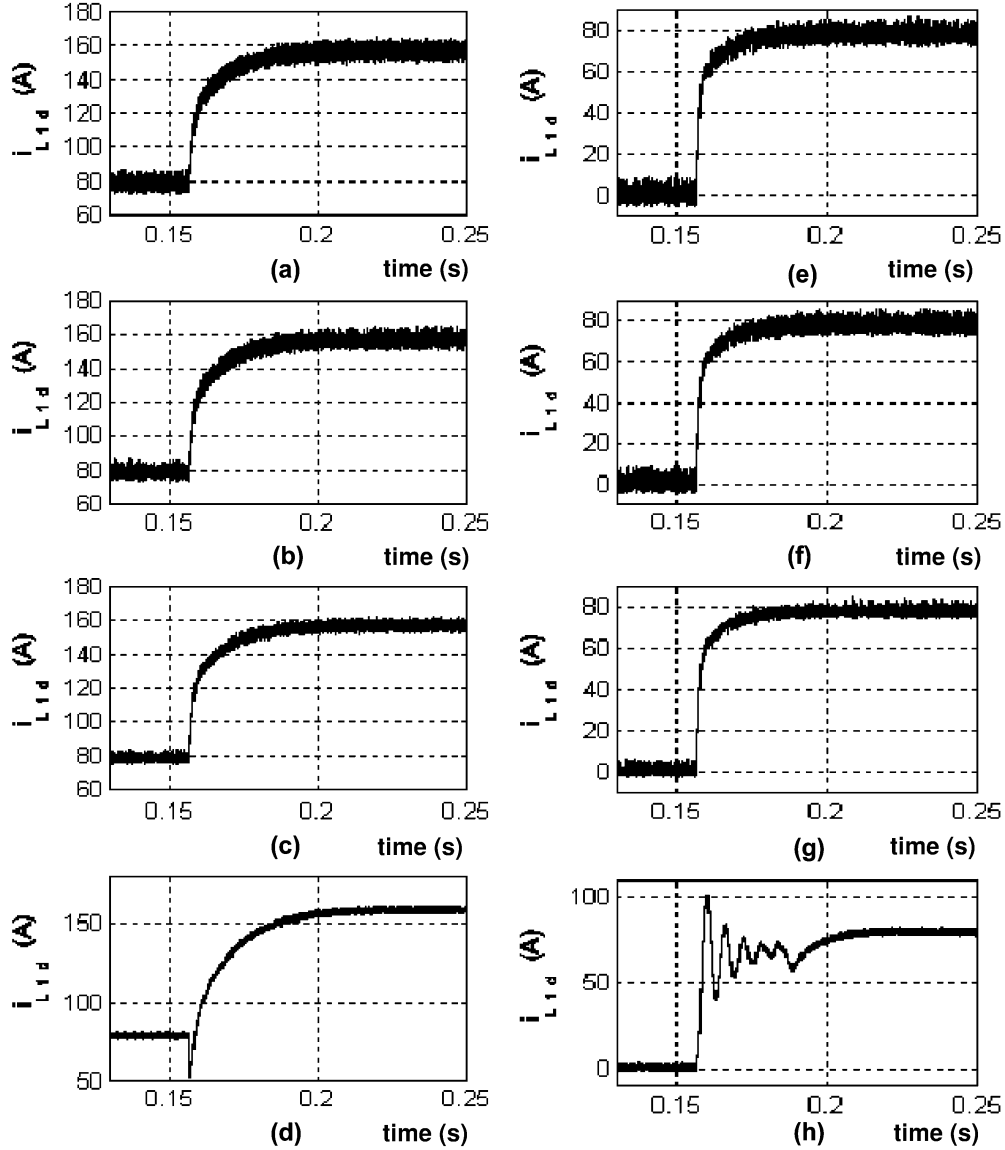


Fig. 9. Change in the active current of M1 obtained using CS_{CONT1} (a), (e), CS_{CONT2} (b), (f), $CS_{DISCRETE}$ (c), (g), and CS_{LINEAR} (d), (h) for *case 1* (figures on the left) and *case 2* (figures on the right).

$$\begin{aligned}
 &= \left(\vec{i}_k^{*dq}(n+1) - \vec{i}_k^{dq}(n+1) \right) - \vec{\sigma}_k^{dq}(n) \\
 &= \left(\vec{i}_k^{*dq}(n+1) - \Phi_k \vec{i}_{L_k}^{dq}(n) + \Gamma_k \vec{V}^{dq} + \Omega_k \vec{t}_k^{dq}(n) \right) \\
 &\quad - \vec{\sigma}_k^{dq}(n) \\
 &= \left(-\lambda_{kd} \text{sgn}(\sigma_{kd}(n)) - \lambda_{kq} \text{sgn}(\sigma_{kq}(n)) \right)^T \quad (24)
 \end{aligned}$$

and then determine $\vec{t}_k^{dq}(n)$. We then use (17) to obtain t_{1k} , t_{2k} , and $t_{0k} = (1/2)(T/2 - t_{1k} - t_{0k})$ from $\vec{t}_k^{dq}(n)$.

While deriving the duration of the zero vectors, we did not distinguish between the vectors U_7 and U_0 . However, to control the zero-axis current, such a distinction is necessary. Let us rewrite the total duration of the zero vectors in a given switching cycle as

$$4t_{0k} = (1 - \beta_k)4t_{0k} + \beta_k(4t_{0k}). \quad (25)$$

It has been shown in [15] that for the PTBR, if $\beta_2 = 0.5$, then by assigning $(1 - \beta_1)4t_{01}$ to U_0 and $\beta_1(4t_{01})$ to U_7 , one can minimize the effect of the zero-axis current. The parameter β_1 is

the output of a feedback loop of M1 that regulates the zero-axis current to zero [15]. If, however, assigning $\beta_2 = 0.5$ is not possible (for reasons of flexibility), then one can obtain the zero vectors as a combination of the active vectors.

IV. RESULTS

We present simulation² results obtained by closing the PTBR using five different controllers. The first one is a conventional linear dq controller [12], [13], while the second one is CS_{LINEAR} [15]. The other three control schemes are CS_{CONT1} , CS_{CONT2} , and $CS_{DISCRETE}$. The values of the nominal parameters for the PTBR are listed in Table I. The outer voltage loop, which regulates the bus voltage at 400 V, has

²The simulation was conducted in Visual Fortran. Although ideal complementary switches are used to simulate the performance of the PTBR (to reduce computational time), a benchmark test using data used to obtain performance results in [13], which uses the same PTBR parameters as in Table I, yielded simulation results which closely follow the steady-state experimental results demonstrated in [13].

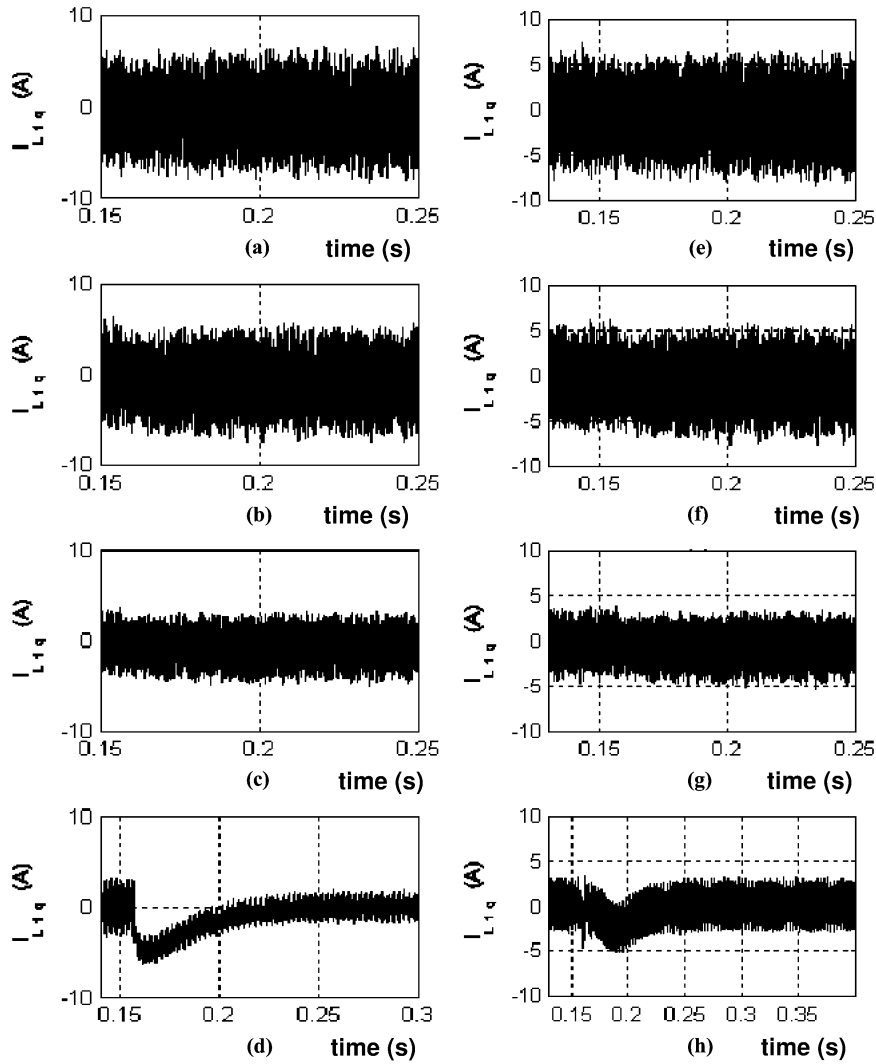


Fig. 10. Change in the reactive current of M1 obtained using CS_{CONT1} (a), (e), CS_{CONT2} (b), (f), $CS_{DISCRETE}$ (c), (g), and CS_{LINEAR} (d), (h) for *case 1* (figures on the left) and *case 2* (figures on the right).

been chosen to have a slower dynamic response as compared to that of the inner current loops to ensure stability of the overall system [16]. The choice of the parameters for the voltage loop is based on the results of [12]. The load is chosen to be resistive in nature and has a magnitude of R . However, the proposed control schemes CS_{CONT1} , CS_{CONT2} , and $CS_{DISCRETE}$ can be applied to systems that involve other types of loads because they are independent of the load type.

In practice, it is impossible to manufacture two identical modules. In fact, it is not uncommon to have variations in the circuit parameters of the order of 5%. To simulate one such scenario, we reduce L_1 by 5% from its nominal value, but keep the values of all of the other parameters of M1 (as well as M2) equal to their nominal values. In Fig. 7(a), we show that, even though there is only a minor difference in one of the parameters of M1 and M2, the phase currents in each module are no more balanced when the PTBR is controlled using a conventional dq controller. In Fig. 7(b), we show projections of the averaged values of the unbalanced phase currents (of M1) in the dqo frame onto the $\alpha\beta o$ axes. It shows that, while the d and q components on the $\alpha\beta$ plane still rotate in a circle, the zero-axis component os-

cillates up and down. Consequently, the load sharing between M1 and M2 is poor. Thus, the performance of a conventional dq control scheme is not satisfactory even under small parametric variations.

In Fig. 7(c), we demonstrate the steady-state performance of the PTBR operating with CS_{LINEAR} [15]. The values of the parameters are the same as those used to obtain Figs. 7(a) and (b). We see that, by controlling the zero-sequence current in addition to the dq currents, the steady-state performance becomes satisfactory. Although the zero-sequence current is not eliminated, its overall effect is minimized.

Next, we explore the dynamic performance of the PTBR using our three proposed control schemes (CS_{CONT1} , CS_{CONT2} , and $CS_{DISCRETE}$) and CS_{LINEAR} under further variations in the parameters of the two modules. The switching frequencies of M1 and M2 are set at 16 and 32 kHz, respectively, to replicate the conditions in [15]. In real life, the two modules will be physically apart and, hence, synchronization of the clocks is expensive and not reliable [13]. Hence, to increase the redundancy of operation, we switch M1 and M2 asynchronously. To test the robustness of CS_{LINEAR} under

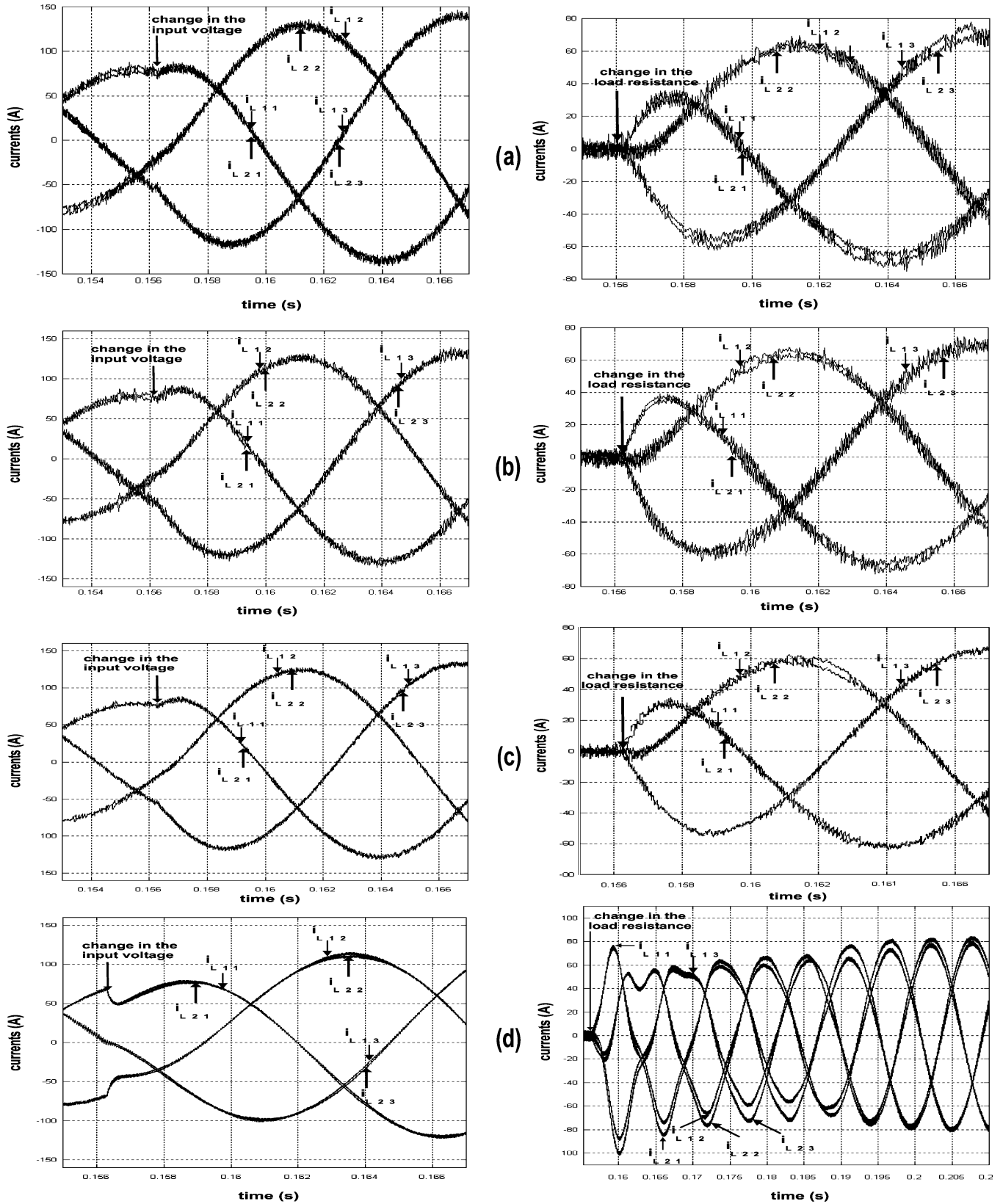


Fig. 11. Distribution of the line currents between M1 and M2 obtained using (a) CS_{CONT1} , (b) CS_{CONT2} , (c) CS_{CONT3} , and (d) CS_{LINEAR} for case 1 (figures on the left) and case 2 (figures on the right). The proposed control schemes and CS_{LINEAR} operate with $L_1 = 85\%L_n$ and $L_1 = 95\%L_n$, respectively.

parametric variation, we reduce L_1 by 5% from its nominal value. We test the robustness of CS_{CONT1} , CS_{CONT2} , and $CS_{DISCRETE}$ by reducing L_1 15%, an even larger variation

in its nominal value. The larger variation in L_1 , which makes paralleling M1 and M2 even more difficult [15], [17], is chosen to test the robustness of the nonlinear controller under extreme

conditions. For all of the control schemes, the values of all of the other parameters are kept equal to their nominal values.

Having set the operating parameters, we determine the response of the PTBR (using CS_{CONT1} , CS_{CONT2} , and $CS_{DISCRETE}$, and CS_{LINEAR}) under small- and large-signal feedforward and feedback disturbances: two cases are considered. For all cases, we investigate the performance of the PTBR by determining the drop in its bus voltage, the change in its reactive and active currents, and the current sharing between the modules.

For case 1, we subject the PTBR, operating in steady state, to a sudden change in the input voltage. Initially, the input voltage is set equal to its nominal value, and after the transient, it is assumed to decrease to 50% of its nominal value. We begin by investigating the drop in the bus voltage. The results are shown in Fig. 8(a)–(d). We find that the dip in the bus voltage is maximum when the PTBR is operated using CS_{LINEAR} ; in addition, recovery time for the bus voltage is longer³. For case 2, we subject the PTBR, operating in steady state, to a sudden change in the load resistance from 400 Ω (almost no load) to 4 Ω (full load). Fig. 8(e)–(h) shows that the changes in the bus voltage obtained using CS_{CONT1} , CS_{CONT2} , and $CS_{DISCRETE}$ are smaller than those obtained with CS_{LINEAR} . Moreover, the recovery time obtained using CS_{LINEAR} is longest. Overall, for either case, the drop in the bus voltage is larger when using CS_{LINEAR} , even though it is implemented for a smaller variation (5%) L_1 as compared to the proposed control schemes (15%).

Next, we investigate the performance of the d -axis (active) current for all cases under feedforward and feedback disturbances. Fig. 9(a)–(d) shows the response of the active current of M1 (i.e., i_{L1d}) for case 1. Later on, we will show the currents of both modules. We see from the figures that, using the proposed control schemes, the PTBR does not have any undershoot after the feedforward disturbance. However, the PTBR shows a significant drop in the i_{L1d} when using CS_{LINEAR} . Because of this undershoot, the drops in the bus voltage obtained using CS_{LINEAR} , as shown in Fig. 8, are higher. The responses of i_{L1d} for case 2, shown in Fig. 9(e)–(h), are self-explanatory and similar to those obtained for case 1. On the whole, although CS_{CONT1} , CS_{CONT2} , and $CS_{DISCRETE}$ operate with a larger variation in L_1 , their performances are good. For case 1, using CS_{LINEAR} , there is more than a 30% undershoot in i_{L1d} immediately after the disturbances. For case 2, the recovery of i_{L1d} using CS_{LINEAR} is not satisfactory.

We then investigate the response of the q -axis (reactive) current of the PTBR for all cases. The results are shown in Fig. 10 for M1. We see that, under steady-state conditions, the average of i_{L1q} obtained using all control schemes is about zero. However, for either a large disturbance in the load or the input voltage, CS_{LINEAR} is unable to maintain the average of i_{L1q} at zero immediately after the disturbance. Therefore, it follows from Figs. 8–10 that, unlike CS_{LINEAR} , the proposed control schemes maintain decoupling between d and q axes

³We also note that the “ripple” in the bus voltage obtained using CS_{CONT1} , CS_{CONT2} , and $CS_{DISCRETE}$ is marginally higher than that obtained with CS_{LINEAR} because they operate with $L_1 = 0.85L_n$ and $L_2 = L_n$ compared to $L_1 = 0.95L_n$ and $L_2 = L_n$ for CS_{LINEAR} . Thus, even with a larger parametric variation, the performances of the proposed control schemes are better than CS_{LINEAR} .

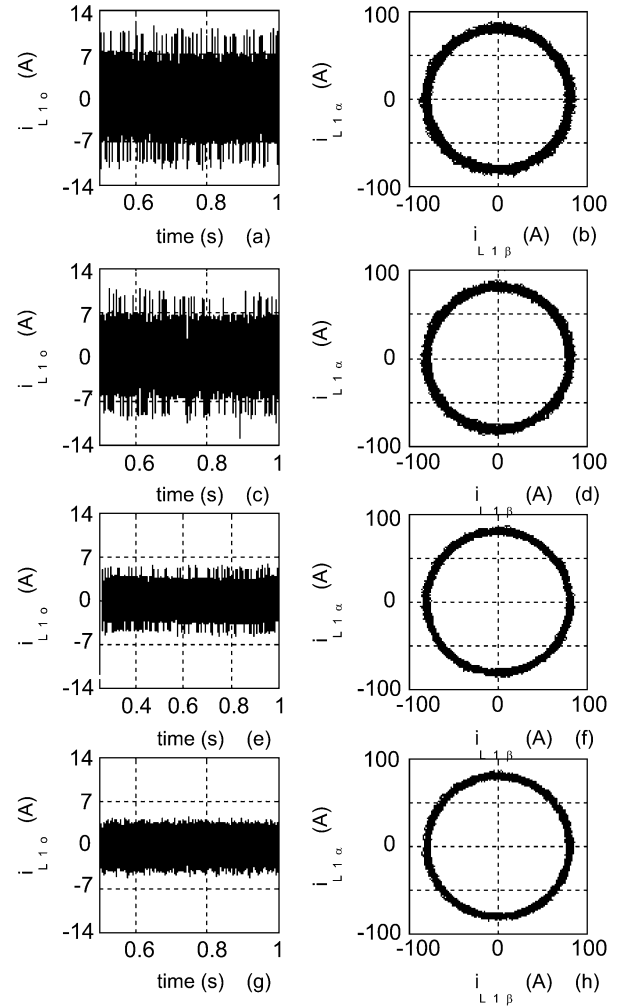


Fig. 12. Steady-state currents on the zero axis and the $\alpha\beta$ axes for M1 obtained using CS_{CONT1} (a), CS_{CONT2} (c), $CS_{DISCRETE}$ (e), (f), and CS_{LINEAR} (g), (h).

even under severe feedforward or feedback disturbances and hence are more robust. Thus, the performances of the proposed control schemes are good, even though they operate with a larger variation in L_1 .

Next, using Fig. 11, we investigate the sharing of the line currents between M1 and M2, when the PTBR is subjected to a large disturbance in either the voltage (case 1) or the load (case 2). For case 1, we see that the best transient response is achieved using CS_{CONT1} ; the response time is comparable to the other two proposed schemes. The recovery time of the PTBR obtained with CS_{LINEAR} is the longest. Moreover, immediately after the change in the voltage, there is an undershoot and an overshoot in two of the phase currents, which are not evident in the responses obtained with the proposed control schemes. For case 2, among the three proposed control schemes, $CS_{DISCRETE}$ achieves the best compromise between the response time and current sharing. The recovery times of CS_{CONT1} and CS_{CONT2} are smaller than that of $CS_{DISCRETE}$. The response of the PTBR obtained with CS_{LINEAR} is significantly inferior to those obtained with the proposed control schemes, both in terms of the response time and current sharing.

Finally, in Fig. 12, we show the impact of the proposed control schemes on the steady-state ripples of the phase

currents (in the $\alpha\beta$ frame) and on the zero-axis current that circulates between the two modules. For all of these plots, we choose $L_1 = 0.85L_n$ and $L_2 = L_n$. All other parameters are kept the same as before. The steady-state ripple obtained with $CS_{DISCRETE}$ is better than those obtained using CS_{CONT1} and CS_{CONT2} . More importantly, the zero-axis current obtained with $CS_{DISCRETE}$ has a smaller magnitude compared to the previous cases. The steady-state results obtained using $CS_{DISCRETE}$ and CS_{LINEAR} are close. Therefore, $CS_{DISCRETE}$ attains the best compromise between the dynamic and steady-state performances.

V. SUMMARY AND CONCLUSION

We have proposed three control schemes to stabilize a PTBR. The first two control schemes (CS_{CONT1} and CS_{CONT2}) are developed in the continuous domain, whereas the third scheme ($CS_{DISCRETE}$) is developed in the discrete domain. The simulation results, with properly tuned controller gains did not exhibit susceptibility to subharmonic instabilities. Control schemes CS_{CONT1} and CS_{CONT2} stabilize the errors on the dq -axes sliding surfaces and rely on blocking the pure zero-sequence current path, the inductor size, and the switching frequency to bind the errors on the zero-axis sliding surfaces. Results show that the transient performances of the PTBR using these two schemes are good. The steady-state ripple of the PTBR obtained using CS_{CONT2} is slightly better than that obtained using CS_{CONT1} , because the former uses a hysteretic comparator, which has an inner and an outer hysteretic band. The steady-state ripple of the PTBR obtained with $CS_{DISCRETE}$ is better than those obtained with the other two proposed control schemes because the former combines SVM and nonlinear control, and stabilizes the zero-axis disturbance as well. Hence, the steady-state ripple has a constant frequency, and the deviation of the zero-axis current from its reference value ($=0$) is minimized.

We also compare the performances of the three proposed controllers with a conventional dq controller [12] and another controller (CS_{LINEAR}), which was recently proposed by Ye *et al.* [15]. We find that the conventional dq controller fails to stabilize the PTBR even for a slight parametric variation of the two modules. This is because the conventional dq controller does not control the current on the zero axis, which is perpendicular to the dq axes. The controller proposed by Ye *et al.* [15] performs better than the conventional dq controller. However, its transient response is inferior to the proposed control schemes for even moderate feedforward and feedback disturbances. For even larger disturbances, the transient performance of the controller proposed by Ye *et al.* [10] suffers considerably.

The effectiveness of CS_{LINEAR} deteriorates under saturated conditions because the zero vectors cannot be applied [15]. Under saturated conditions, $CS_{DISCRETE}$ shares the same limitation as CS_{LINEAR} . However, unlike the latter, the proposed controller guarantees global stability within the boundary layer [16]. That is why its transient performances are better. The proposed control schemes, developed in the continuous domain, do not have any such limitations, but create more harmonic distortions. Therefore, to obtain a balance between

steady-state and transient performances and to operate the PTBR in saturated conditions, a combination of CS_{CONT1} or CS_{CONT2} (outside the boundary layer) and $CS_{DISCRETE}$ (inside the boundary layer) is recommended. Implementation of such a hybrid control scheme on a digital signal processor is fairly straightforward. However, if the worst case disturbances are not large enough to saturate the PTBR, then $CS_{DISCRETE}$ provides the best alternative.

APPENDIX

MATRICES $P_{ki}(i = 1, 2, \dots, 5)$

$$\begin{aligned}
 P_{11} &= -\frac{rL_1}{3L_1(L_1 + L_2)} \\
 &\quad \times \begin{bmatrix} 3L_1 + 2L_2 & -L_2 & -L_2 \\ -L_2 & 3L_1 + 2L_2 & -L_2 \\ -L_2 & -L_2 & 3L_1 + 2L_2 \end{bmatrix} \\
 P_{12} &= -\frac{rL_2}{3(L_1 + L_2)} \begin{bmatrix} 1 & 1 & 1 \\ 1 & 1 & 1 \\ 1 & 1 & 1 \end{bmatrix} \\
 P_{13} &= \frac{1}{3L_1} \begin{bmatrix} 2 & -1 & -1 \\ -1 & 2 & -1 \\ -1 & -1 & 2 \end{bmatrix} \\
 P_{14} &= -\frac{1}{6L_1(L_1 + L_2)} \\
 &\quad \times \begin{bmatrix} 3L_1 + 2L_2 & -L_2 & -L_2 \\ -L_2 & 3L_1 + 2L_2 & -L_2 \\ -L_2 & -L_2 & 3L_1 + 2L_2 \end{bmatrix} \\
 P_{15} &= \frac{1}{6L_1(L_1 + L_2)} \begin{bmatrix} L_1 & L_1 & L_1 \\ L_1 & L_1 & L_1 \\ L_1 & L_1 & L_1 \end{bmatrix} \\
 P_{21} &= -\frac{rL_1}{3(L_1 + L_2)} \begin{bmatrix} 1 & 1 & 1 \\ 1 & 1 & 1 \\ 1 & 1 & 1 \end{bmatrix} \\
 P_{22} &= -\frac{rL_2}{3L_2(L_1 + L_2)} \\
 &\quad \times \begin{bmatrix} 3L_2 + 2L_1 & -L_1 & -L_1 \\ -L_1 & 3L_2 + 2L_1 & -L_1 \\ -L_1 & -L_1 & 3L_2 + 2L_1 \end{bmatrix} \\
 P_{23} &= \frac{1}{3L_2} \begin{bmatrix} 2 & -1 & -1 \\ -1 & 2 & -1 \\ -1 & -1 & 2 \end{bmatrix} \\
 P_{24} &= \frac{1}{6L_2(L_1 + L_2)} \begin{bmatrix} L_2 & L_2 & L_2 \\ L_2 & L_2 & L_2 \\ L_2 & L_2 & L_2 \end{bmatrix} \\
 P_{25} &= -\frac{1}{6L_2(L_1 + L_2)} \\
 &\quad \times \begin{bmatrix} 3L_2 + 2L_1 & -L_1 & -L_1 \\ -L_1 & 3L_2 + 2L_1 & -L_1 \\ -L_1 & -L_1 & 3L_2 + 2L_1 \end{bmatrix}.
 \end{aligned}$$

REFERENCES

- [1] D. Milosavljevic, "General conditions for the existence of a quasisliding mode on the switching hyperplane in discrete variable structure systems," *Autom. Remote Control*, vol. 46, pp. 307–314, 1985.

- [2] K. Matsui, "A pulsewidth modulated inverter with parallel-connected transistors by using current sharing reactors," in *Conf. Rec. IEEE-IAS Annu. Meeting*, 1985, pp. 1015–1019.
- [3] I. Takahashi and M. Yamane, "Multiparallel asymmetrical cycloconverter having improved power factor and waveforms," *IEEE Trans. Ind. Appl.*, vol. 22, no. 6, pp. 1007–1016, Nov./Dec. 1986.
- [4] S. Ogasawara, J. Takagaki, H. Akagi, and A. Nabae, "A novel control scheme of duplex current-controlled PWM inverters," in *Conf. Rec. IEEE-IAS Annu. Meeting*, 1987, pp. 330–337.
- [5] T. Kawabata and S. Higashino, "Parallel operation of voltage source inverters," *IEEE Trans. Ind. Appl.*, vol. 24, no. 2, pp. 281–287, Mar./Apr. 1988.
- [6] V. D. Broeck, H. C. Skudelny, and G. Stanke, "Analysis and realization of a pulse width modulator based on voltage space vectors," *IEEE Trans. Ind. Appl.*, vol. 1, pp. 142–150, Jan./Feb. 1988. IA-24.
- [7] J. W. Dixon and B. T. Ooi, "Series and parallel operation of hysteresis current-controlled PWM rectifiers," *IEEE Trans. Ind. Appl.*, vol. 25, no. 4, pp. 644–651, Jul./Aug. 1989.
- [8] Z. Zhang and B. Ooi, "Multimodular current-source SPWM converters for superconducting a magnetic energy storage system," *IEEE Trans. Power Electron.*, vol. 8, no. 3, pp. 250–256, May 1993.
- [9] N. S. Behilovic, T. Ninomiya, A. Sabanovic, and B. Perunicic, "Control of three-phase switching converters: A sliding mode approach," in *Proc. IEEE PESC'93*, 1993, pp. 630–635.
- [10] Y. Komatsuzaki, "Cross current control for parallel operating three-phase inverter," in *Proc. IEEE PESC'94*, 1994, pp. 943–950.
- [11] Y. Sato and T. Kataoka, "Simplified control strategy to improve ac input-current waveform of parallel connected current-type PWM rectifiers," *Proc. Inst. Elect. Eng.*, vol. 142, pp. 246–254, 1995.
- [12] S. Hiti, "Modeling and control of three-phase PWM converters," Ph.D. dissertation, Dept. Elect. Comput. Eng., Virginia Polytechnic Inst. State Univ., Blacksburg, 1995.
- [13] K. Xing, F. C. Lee, D. Boroyevich, Z. Ye, and S. K. Mazumder, "The circulating current in paralleled three-phase boost PFC rectifiers," *IEEE Trans. Power Electron.*, vol. 14, no. 5, pp. 250–256, Sep. 1999.
- [14] J. F. Silva, "Sliding-mode control of boost-type unity-power-factor PWM rectifiers," *IEEE Trans. Ind. Electron.*, vol. 46, no. 3, pp. 594–603, Jun. 1999.
- [15] Z. Ye, D. Boroyevich, J. Y. Choi, and F. C. Lee, "Control of circulating current in parallel three-phase boost rectifiers," in *Proc. IEEE APEC'00*, vol. 1, 2000, pp. 506–512.
- [16] S. K. Mazumder, "Nonlinear analysis and control of standalone, parallel dc-dc, and parallel multi-phase PWM converters," Ph.D. dissertation, Dept. Elect. Comput. Eng., Virginia Polytechnic Inst. State Univ., Blacksburg, 2001.
- [17] S. K. Mazumder, "A novel discrete control strategy for independent stabilization of parallel three-phase boost converters by combining space-vector modulation with variable-structure control," *IEEE Trans. Power Electron.*, vol. 18, no. 4, pp. 1070–1083, Jul. 2002.



Sudip K. Mazumder (SM'04) received the Ph.D. degree in electrical and computer engineering from Virginia Polytechnic Institute and State University, Blacksburg, in 2001.

Currently, he is an Assistant Professor in the Department of Electrical and Computer Engineering, University of Illinois, Chicago. He is also the Director of the Laboratory for Energy and Switching-Electronics Systems. He has over ten years of professional experience and has held R&D and design positions in leading industrial organizations. His areas of expertise and current interests include stability analysis of interactive power-electronic networks (IPNs) and wireless control of IPNs, fuel-cell-based power-electronics systems and analysis of the electrical-feedback effects of power electronics on fuel cells, optically switched power conversion, self-powered wireless sensors, advanced control and DSP/RISC- and ASIC-based embedded controllers for power supplies/systems and motor drives, and soft- and hard-switching topologies and techniques in power converters. He has published 40 refereed and invited journal and conference papers and is a Reviewer for six international journals.

Dr. Mazumder received the U.S. Department of Energy SECA and National Science Foundation CAREER Awards in 2002 and 2003, respectively. He also received the Prize Paper Award from the IEEE TRANSACTIONS ON POWER ELECTRONICS and the IEEE Power Electronics Society in 2002. He is an Associate Editor of the IEEE TRANSACTIONS ON INDUSTRIAL ELECTRONICS and IEEE POWER ELECTRONICS LETTERS and is listed in *Who's Who in Engineering Education*. In the summer of 2004, he was a Faculty Fellow at the Pacific Northwest National Laboratory (PNNL) and a Panel Reviewer for the National Science Foundation.